RSC Advances

ROYAL SOCIETY OF CHEMISTRY

www.rsc.org/advances

RSC Advances

RSCPublishing

ARTICLE

Rotating Disk Slurry Electrodeposition of Platinum at Y-Zeolite/Carbon Vulcan XC-72R for Methanol Oxidation in Alkaline Media

Amal Suleiman [a], Christian L. Menéndez [a], Ramón Polanco,[b] Esteban Rosim Fachini,[c] Yaritza Hernández-Lebrón[a], Maxime J-F Guinel[a, d], Rolando Roque-Malherbe[*,b] and Carlos R. Cabrera[*,a]

Cite this: DOI: 10.1039/x0xx00000x

Platinum was electrodeposited onto Y-zeolite and Y-zeolite(Y)/Vulcan XC-72R(V) to produce Pt/Y/V and Pt/Y catalysts using a rotating disk slurry electrode technique. The activities of the two catalysts were measured towards methanol electro-oxidation in alkaline media by cyclic voltammetry and chronoamperometry. The materials were examined using electron microscopy. The results were compared to those obtained on commercial catalysts. Pt/Y/V (with 14 wt.% Pt) catalyst was the most active, even so more than a commercial Pt/V catalyst with 20 wt. % Pt. The Pt/Y/V catalysts contained Pt nanoparticles and tetrahedron, likely a consequence of the nucleation and growth within the zeolite framework.

Received 00th June 2014,
Accepted 00th June 2014

DOI: 10.1039/x0xx00000x

www.rsc.org/

1. Introduction

Efforts are made to develop the direct electrochemical oxidation of alcohol and hydrocarbon fuels as an energy source.[3, 4, 5] In particular, methanol has been largely investigated, since it is cheap, can be produced from fossil fuels or sustainable sources, and can be delivered the same way used today for petroleum.[6] However, the commercial expansion of this fuel cell type depends largely on the catalysts since they are expensive and show unstability during long operation periods.[7]

Direct methanol fuel cell (DMFC) is a variety of the polymer electrolyte fuel cell, conformed by a polymeric membrane that separates the anode and the cathode electrodes where methanol is used as a liquid fuel.[8,9,10,11] The operation of the cell can produce catalyst loss by corrosion, catalyst particles sintering and catalyst poisoning.[12] Therefore, having highly dispersed nanoparticles on conductive high surface area supports may improve the stability and robustness of the catalytic process. In this direction, efforts are made preparing highly dispersed catalysts on carbon based supports such as carbon black (Carbon Vulcan XC-72R)[13, 14] carbon nanotubes[15,16] ordered porous carbon[17], carbon nano-onions[14], nanodiamond[18], among others.[7]

Platinum, in general, is the most active catalysts[11]. However, in order to efficiently use platinum as catalyst the metal must be highly dispersed in the form of small nanoparticles, since, with ultra-low loadings [4,7], therefore, reducing the total cost of the catalyst.[19]

Aluminosilicate zeolites supports have been used in methanol and CO oxidation as well as for the water-gas-shift reaction.[20,21,22] Their structure, composition and properties that offer an elevated ionic strength environment. Rolison has shown the use of these materials in electrochemistry.[23,24,25] The properties of aluminosilicate zeolites responsible for affecting charge transfer reactions in electrochemical systems[23] are, the zeolite size and shape selectivity due to their rigid pores and channels, the ion exchange properties, and their catalytic properties. In this regard, hydrated zeolites conduct through intracrystalline and intercrystalline cationic conduction, given that, the material behave as an electrolyte, by the water adsorbed in the primary and secondary porosity of the zeolite[26]. On this ground, in the formulation of the electro-catalyst included in the DMFC is possible to incorporate an additional component, namely an aluminosilicate zeolite,[27] since this material in an aqueous electrolyte solution may work as a solid ion conductor[28], provide an adsorption space[29] and supply ions by ionic exchange.[30,31]

The tested metallic catalysts were produced by electrochemical reduction of platinum from K_2PtCl_6on the plain zeolite and a zeolite-carbon black composite, using the rotating disk-slurry electrode (RoSDE) technique. The produced catalysts were compared with

three standard commercial catalysts, specifically, Pt-black, 20 wt. % Pt/Vulcan XC-72R (ETEK) and 40 wt. % Pt/Vulcan XC-72R (ETEK) catalysts. The materials were examined using scanning and transmission electron microscopy (SEM, TEM), , thermo-gravimetric analysis (TGA), powder X-ray diffraction (PXRD), Inductive Couple Plasma – Optical Emission Spectrometry (ICP-OES), X-ray photoelectron spectrometry (XPS), diffuse reflectance Fourier transform infrared spectrometry (DRIFTS), and carbon dioxide adsorption. Finally, the electrochemical measurements were done for methanol oxidation in alkaline media.

2. Experimental method

2.1 Materials

All the chemicals were analytical grade without additional purification. The water used in the synthesis process was bi-distilled. Vulcan XC-72R (Cabot) and zeolite Na-Y (Si/Al = 2.4) (Sigma-Aldrich) were used as support materials. The Vulcan was sonicated in 1.0M H_2SO_4 for 8 h previous to be used to increase the oxygen in the surface of the carbon black particles and disperse it in the slurry. The zeolite was treated for the dealumination process and to exchange Na^+ by H^+ ions.[30, 33]

The electro-deposition of the platinum nanoparticles was performed using the rotating disk-slurry electrode (RoDSE) methodology, following a procedure previously developed in a three compartments, separated by fritted glass, electrochemical cell. The cell was composed of a rotating disk electrode (RDE) (PINE Instrument Company) in the central section, a graphite rod, was used as counter electrode, and a Ag/AgCl (+0.197 V versus NHE) (PINE Instrument Company) was the reference electrode, both in aqueous sulfuric acid solution (0.1 M), included in the right and left sectors of the cell respectively. The disk electrode was a glassy carbon electrode (Bioanalytical System) with an area of 0.20 cm^2. The commercial catalysts used to compare the activity of the Pt/Y/V catalysts were Pt black (Johnson Matthey, high surface area), 20 wt. % Pt/Vulcan XC-72R (ETEK) and 40 wt. % Pt/Vulcan XC-72R (ETEK).

2.2 Catalyst preparation using the RoDSE electrodeposition technique

The procedure used for the preparation of the Pt/Y/Vulcan (Pt/Y/V) and Pt/Y catalysts was used as reported by Santiago et al.[13] Figure 1 shows a scheme of RoDSE process where metal precursor is dissolved into dispersed in a slurry solution of a colloidal support, and an electrodeposition potential is applied to the RDE while rotating at 900 rpm. Briefly, a concentrated suspension was formed with 50 mg of zeolite in 20 ml of 0.1M H_2SO_4, this slurry was placed in the center of the three-electrode cell assembly for the platinum electro-deposition. Then 5.00 mL of the 3 mM K_2PtCl_6 (Aldrich) was added to the suspension in the center compartment to make the slurry solution. The electrochemical cell was sealed, and purged with nitrogen for 1 h, while the RDE was rotated at 900 rpm in the slurry. The electro-deposition took place at a constant potential, -0.200 V vs. Ag/AgCl (Basic Electrochemical System of EG&G) for 2 h. The electro-deposition was repeated six additional times (i.e. 6 x 2hrs)while adding the platinum complex solution (5.00 mL of 3 mM K_2PtCl_6). Figure 1 shows an illustration of the electrodeposition technique describe above. Afterwards, the slurry was filtered and rinsed with 600 mL of nanopure dionized water (18.2 MΩ-cm NANOpure Diamond of Barnstead) to remove the impurities. The filtered sample was air-dried. For the Pt/ Y/ V catalyst preparation, slurry of 50 mg of Vulcan-Zeolite (1:1) in 20 mL of 0.1M H_2SO_4 was placed in the center of the three-electrode cell assembly for the platinum electro-deposition. Afterwards, the methodology was repeated for the preparation of the Pt/Y sample.

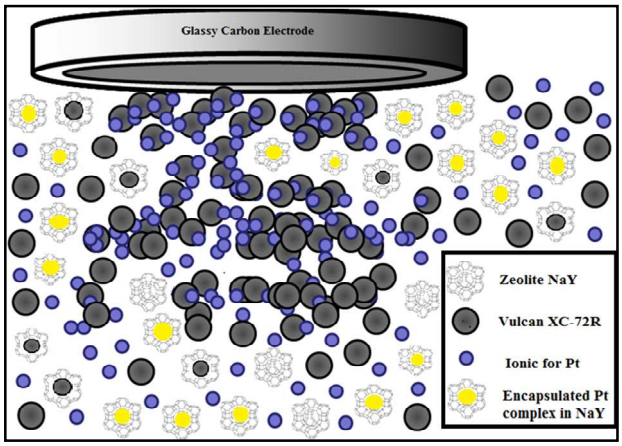

Fig. 1. Schematic illustration of the RoDSE technique process.

2.3 Preparation of catalyst coated glassy carbon (GC) electrodes

To produce the ink-paste-electrode (IPE), a suspension containing 1.0 mg of the catalytic nanomaterial, 100 µL of nano-pure water and 200 µL of isopropanol was placed under ultrasound for 30 minutes. Then, 8 µL of Fumion® (5 % w/w polyarylene sulfonic acid polyelectrolyte dissolved in water/isopropanol, FuMA-Tech GmbH, St. Ingbert, Germany) was added and stirred for 30 minutes. The electrode was prepared by adding 8 µL of the ink paste to the glassy carbon electrode (3 mm diameter, Bioanalytical System) and then air dried for 30 minutes.

2.4 Characterization methods

The samples were examined using two scanning electron microscopes (SEM, JEOL, JSM-7500F and JSM-6480LV). . The catalysts were also investigated using a high resolution transmission electron microscope (HRTEM, JEOL, JEM-2200FS). The elemental composition of the Pt/Y/Vulcan XC-72R catalyst was measured using Perkin Elmer Inductively Coupled Plasma-Optical Emission Spectrometer (ICP-OES) Optima 8000.

X-ray photoelectron spectroscopy (XPS) (PHI 5600ci) surface analysis was done using an Al Kα monochromatic X-ray source (350 W) and a hemispherical electron energy analyzer. The analysis was made pressing the catalytic powder onto a Mo film.

Powder X-ray diffraction (PXRD) (Bruker D8 Advance) profiles were collected using a Bragg- Brentano vertical goniometer configuration. The thermal gravimetric analysis (TGA) (TA, Q-500) measurements were done from 25 to 700 ^0C, at a heating rate of 5 ^0C /min, while flowing 100 ml/min of pure N_2. Diffuse reflectance infrared Fourier transform spectroscopy (DRIFTS) was done by using a Thermo Scientific Nicolet iS10 FTIR spectrometer. The data were collected at a resolution of 4 cm^{-1} employing 100 scans per sample. A background, with pure KBr, provided by Nicolet, using the same conditions was always made prior to sample analysis. The hydrated samples spectra were obtained at room temperature under N_2 flow (Praxair, 99.99 %), at 50 ml/min rate. The spectra of the dehydrated samples was done by heating at 473 K under a 50 ml/min flow of N_2 (Praxair, 99.99 %) for 2 hours.

The spectra of the degassed materials were subsequently obtained at room temperature, under N_2 flow. Additionally, DRIFTS spectra of carbon dioxide (Praxair, 99.99 %) adsorbed in the Pt/Y/V catalyst were obtained utilizing as background the dehydrated sample at room temperature. After that, CO_2 (Praxair, 99.99 %) flow at a 50 ml/min rate, for three minutes, was passed through the dehydrated samples, afterward, the sample was purged under N_2 (Praxair, 99.99 %) flow at a rate of 50 ml/min for one minute, next, a spectrum of the carbon dioxide molecule adsorbed on the catalyst was obtained at room temperature under N_2 flow.
Carbon dioxide (Praxair, 99.99 %) adsorption[19] at 273 K and pressure up to ca. 1 atm. on samples degassed at 473 K for three hours under high vacuum (10^{-6} Torr), was carried out using an upgraded Quantachrome Autosorb-1 automatic volumetric physisorption analyzer. The backfilling process was carried out using helium (Praxair, 99.99 %).

2.5 Cyclic voltammetry and constant potential experiments

The electrochemical activity of the catalysts were measured using a potentiostat/galvanostat system (EG&G) and a three electrode compartment electrochemical cell, separated by glass frits.[13,14] The potentials measured in this study were referenced to Ag/AgCl. The cyclic voltammetric (CV) experiments of the tested catalysts were done in 0.1 M KOH using a potential range of between −0.9 and 0.6 V vs. Ag/AgCl and a potential sweep rate of 100 mV/s at room temperature. The counter electrode was a Pt wire. All electrolyte solutions were bubbled with argon gas for 10 min. before use. The Pt active surface areas were calculated from the cyclic voltammograms in 0.1 M KOH solutions using the hydrogen adsorption/desorption region. In addition, the activity of the Pt/Y/V catalyst towards methanol oxidation in basic media, 1.0 M methanol and 0.1 M KOH, was done and compared against that of Pt black and 40 % Pt/Vulcan XC-72R (ETEK) catalysts.
The onset potential for each catalyst was determined at 5 % of the maximum anodic peak current density for the methanol oxidation reaction. The chronoamperometry experiment was done with an applied potential of -0.4 V vs. Ag/AgCl in 1.0 M methanol and 0.1 M KOH aqueous solution at room temperature.

2.6 CO stripping experiment
To perform CO oxidative stripping experiments in alkaline medium, the ink paste electrodes were placed in a solution of 0.1 M KOH. Then, CO adsorption on the Pt surface was done by bubbling high purity CO through the working electrode cell compartment for 1200 seconds at a constant applied potential of -0.7 V vs. Ag/AgCl. Afterward, N_2 was bubbled for 300 seconds at the same potential to remove any remaining CO present in solution. The final step was a linear sweep voltammetry (LSV) from -0.7 V to 0.7 V vs. Ag/AgCl at a sweep rate of 20 mV/s.

3. Results and discussion

3.1 Morphology and structure of the catalysts

The structure and chemical identity of Pt/Y/V were verified by the SEM, HRTEM and XRD studies. All the SEM images present nearly cubic zeolite crystals.30 In figure 2, the platinum nanoparticles appear brighter. At the same time as the SEM study, an EDAX elemental analysis of the as-synthesized catalysts was done in five different spots. The weight percent (wt. %) average values were 27 % platinum, 12 % oxygen, 7.6 % silicon and 53 % carbon.

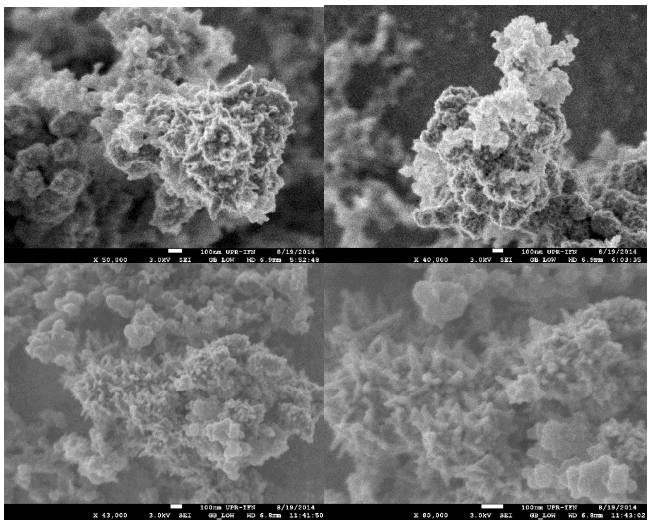

Fig. 2. Scanning electron microscopy images of the Pt/Y/V catalysts prepared by RoDSE.

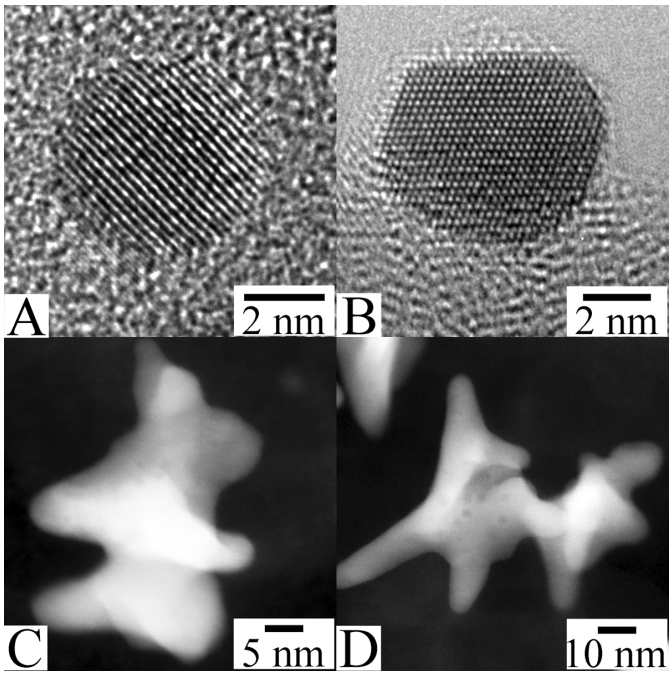

Fig. 3. TEM images showing the Pt crystallites in the Y/V catalyst.

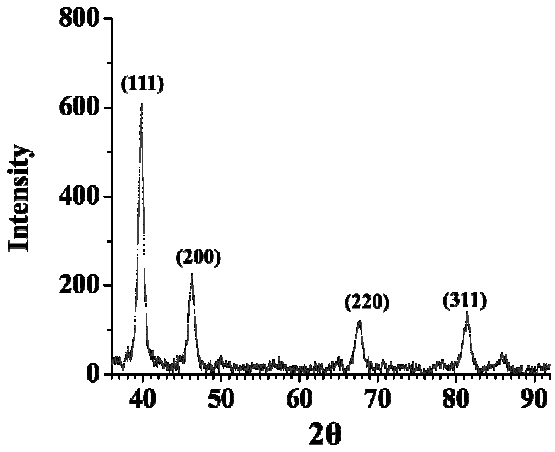

Fig. 4. X-ray diffraction of the Pt/Y/V sample prepared by RoDSE.

The structure and chemical identity of Pt/Y/V were verified by HRTEM and XRD studies. The prepared sample by RoDSE technique was characterized by high resolution transmission electron microscope to detect if the platinum were deposited onto the carbon/zeolite support. High resolution TEM images showing platinum nanostructures are displayed in Fig. 3. The nanoparticles measured in HRTEM had a particle size of 4 to 9 nm. Image 3a and 3B shows Pt nanoparticles. This is likely a result of the nucleation of Pt on the carbon Vulcan XC-72R. Images 3C and 3D show Pt tetrahedron nanostructures. This is likely a result of the nucleation of Pt in the framework of the zeolite. XRD data suggested that there were 8 (1) nm nanoparticles of Pt. The XRD pattern (Fig. 4) shows the face-centered cubic crystal structure of Pt with the presence of (111), (200), (220), (311) and (222) planes, demonstrating highly polycrystalline structure.

The contribution of an addition of Vulcan XC-72R to Pt/HY was the ability to carry or conduct an electrical current and to avoid segregation or agglomeration of Pt. The presence and distribution of platinum, Vulcan and zeolite in this catalyst is confirmed by EDX elemental mapping analysis shown in Fig. 5.

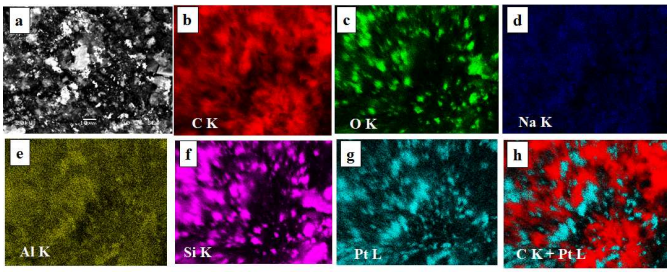

Fig. 5. (a) Field emission electron microscopy images of the Pt/Y/V catalyst on a carbon tape. EDX elemental mapping of (b) carbon(red), (c) oxygen (green), (d) sodium (dark blue), (e) aluminum (yellow), (f) silica (pink), (g) platinum (cyan) of the catalyst in (a). (h) Combined mapping image of both C and Pt.

Fig. 6a presents X-ray photoelectron spectroscopy (XPS) spectrum of the Pt 4f binding energy region corresponding to the as-synthesized Pt/Y/V.[35] Fig. 6b and 6d are exhibited the O 1s[36] and C1s[37] binding energy regions of the XPS profiles. Further, in Fig. 6d is displayed the XPS peak corresponding to the Si 2p.

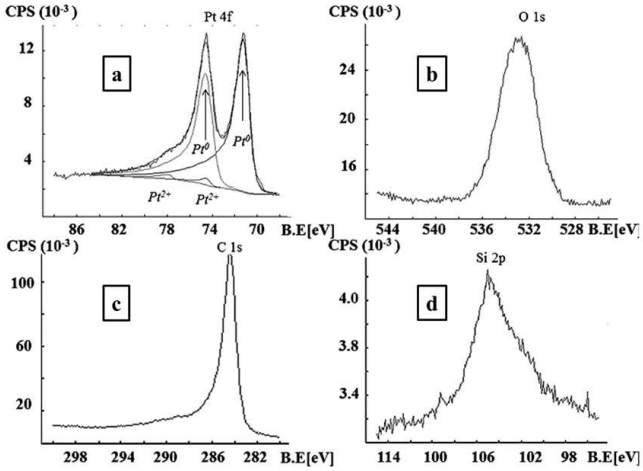

Fig. 6. X-ray photoelectron spectroscopy profiles corresponding to the as-synthesized Pt/Y/V catalyst.

XPS showed a composition of 17.0 % platinum, 9.11% oxygen, 4.17% silicon, 69.25% carbon and 1.0% chlorine on the surface of sample.

High resolution XPS spectra for the Pt 4f binding energy peak were analyzed to identify the platinum oxidation states on the prepared sample by the RoDSE technique. The XPS binding energy data revealed that the majority of the platinum was in its metallic form[26,27] in the Pt/ Y/ V catalyst (Fig. 6a), i.e., the RoDSE Pt electrodeposition process was highly efficient. Figure 6a shows the curve-fitting analysis for the Pt/Y/V sample, which appear to have two different platinum species, Pt (0) and Pt (II). The first set of XPS doublets in the binding energy of 71.3 (55.46% area) and 74.6 (41.6 % area) eV is the most intense and correspond to Pt (0) followed by Pt (II) which is less intense and corresponds is found at 74.5 (1.69 % area) and 77.9 (1.27% area) eV. The appearances of these two platinum species were as expected because of the use of Pt complex as a precursor. On the other hand, the peak in the C 1s binding energy region correspond to graphitic carbon.[37]

In Fig. 7 are exhibited the XRD profiles of the Pt/Y/V and commercial catalysts samples at room temperature. These XRD profiles were resolved into separate Bragg components using the Pawley whole-powder pattern decomposition method while the cell parameter was refined[38] knowing that platinum crystallizes in the cubic $Pm\bar{3}m$ space group. Besides, the Gaussian crystallite size (φ_{Pt}) was calculated.

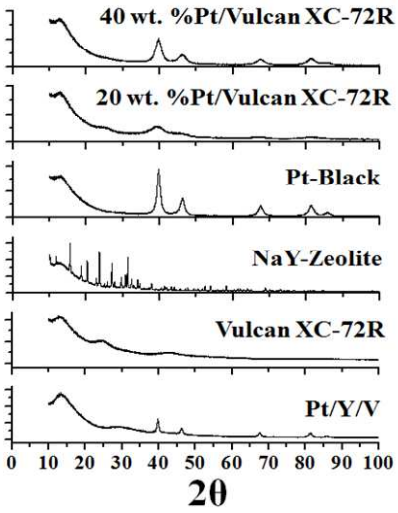

Fig. 7. X-ray diffraction profiles of the Pt/Y/V,Vulcan XC-72R, NAY zeolite, Pt Black, 20 %Pt/Vulcan XC-72R and 40 % Pt/Vulcan XC-72R.

The computer program used to perform these calculations was the Bruker DIFFRAC*plus* TOPAS™ software. The calculated Gaussian crystallite size is 5(1) nm 40 wt. % Pt/Vulcan XC-72R, 4(1) nm 20 wt. % Pt/Vulcan XC-72R, 7(1) nm Platinum black and 8(1) nm Pt/Y/V. Subsequently, to verify the loss of the guest molecules (fundamentally H_2O) throughout heating and study further structural features, the thermal gravimetric analysis (TGA) method was used (Fig. 8).[38]

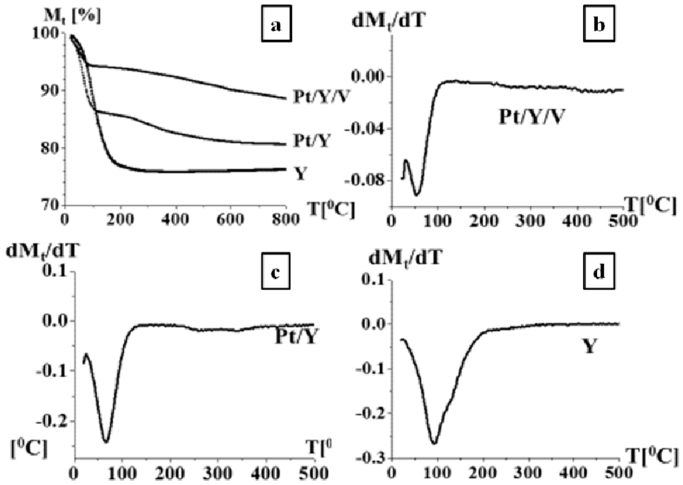

Fig. 8. Thermal gravimetric analysis (TGA) profiles (a) and TGA derivative profiles of Pt/Y/V (b), Pt/Y (c) and Y zeolite (d).

The TGA profile of the Pt/Y/V and Pt/Y catalysts and the Na-Y zeolite are exhibited in Fig. 8a. Meanwhile, in Fig. 8b, 8c and 8d are reported the TG profile derivatives of both catalysts and the zeolite. These results indicated that adsorbed water was released from ca. 50 to 200 ^{0}C. Afterwards, zeolite dehydroxylation from ca. 200 to 700 ^{0}C was produced[42], next, was evidenced the characteristic slight decrease of weight from 200 to 700 ^{0}C, normally observed in carbon black.[43] Further, with the TGA data were calculated the amount of platinum contained in the Pt/Y/V and Pt/Y catalysts, by the comparison of the water weight lost by the pure zeolite Y, the Y/Pt/V, and the Pt/Y catalysts, namely, 0.24 g/g, 0.08g/g and 0.23 g/g. With this information was estimated that, ca. 0.40 ± 0.03 g/g of zeolite Y and 0.40 ± 0.03 g/g of Vulcan were contained in the Pt/Y/V catalyst, since by design the proportion of zeolite Y and Vulcan was 1:1. On this ground, the amount of platinum in the Pt/Y/V catalyst was, 0.19 ± 0.06 g/g, while the amount of Pt in the Pt/Y catalyst was, 0.1 ± 0.02 g/g. The ICP data showed the amount of Pt 14.7%, Si 32.2%, Na 0.59%, Al 0.61%, and the remaining 51.9% was carbon, oxygen, and nitrogen. From the ICP data we see a slightly lower value than the TGA data. Nevertheless, the ICP data confirms the dealuminization process when placing the NaY in 0.1M H_2SO_4 and that the Pt electrodeposition is possible at NaY/Vulcan using the RoDSE technique. Finally, the small amount of Na is indicative that an ion exchange with H^+ and Pt complex during the sonication and electrodeposition process. Cosequently, the zeolite include in the catalyst is in the acid form that is HY zeolite. In the presence of Pt complex in the acid solution may have had an intercalation process in the zeolite framework leading to the Pt tetrahedral formation (see Figure 3C & 3D).

An estimation of the chemical surface area (S_{CSA}) of the platinum phase included in the produced, Pt/Y/V, Pt black and the commercial catalysts ETEK (40% Pt/Vulcan XC-72R) was made, using the following relation, $S_{CSA} = 6/\Phi\rho$. In this regard knowing that the measured crystallite size was, 4 to 9 nm for the Pt/Y/V catalysts respectively and the platinum density, ρ = 21.5 g/cm^3, then is possible the estimation of S_{CSA} for the produced catalysts. The chemical surface area of Pt/Y/V is between 30 m ^{2}/g to 70 m ^{2}/g. Besides, using data previously published[44], namely, S_{CSA} for the 40 % Pt/Vulcan XC-72R ETEK was 111 m ^{2}/g, whereas, the specific surface area of the Pt black was 28 m ^{2}/g. [45]

Later, the DRIFTS spectra of the hydrated (as-synthesized) and dehydrated Pt/Y/V in the range between: 600-3900 cm^{-1} were collected (Fig. 9a). The main IR active vibrations observed can be classified in two main regions. In the first expanse, from 600 to 2000 cm^{-1}, appear bands corresponding to the zeolite structure, meanwhile the second section of the spectrum, namely, between 3200-3700 cm^{-1}, display the stretching, $\nu(OH)$ vibration produced by adsorbed water.[31] Further, the DRIFTS spectrum of the Pt/Y/V catalyst, dehydrated at 200 ^{0}C in N_2 flow, is exhibited in Fig. 9b. This spectrum exhibit a peak at ca. 3605 cm^{-1} related with bridging acid hydroxyl (Si-OH-Al) groups, and displays a very small band at ca. 3700 cm^{-1}, corresponding to the silanol (Si-OH) groups.[44] The acid sites were produced by the electro-deposition, since this process was performed in acid media, therefore, as was previously stated, the Na^+ ions included in the Na-Y zeolite were exchanged by H^+, producing the detected bridging acid hydroxyl (Si-OH-Al) groups. Furthermore, the DRIFTS spectrum of carbon dioxide, adsorbed at 760 Torr on the deshydrated Pt/Y/V can be examined in Fig. 10.

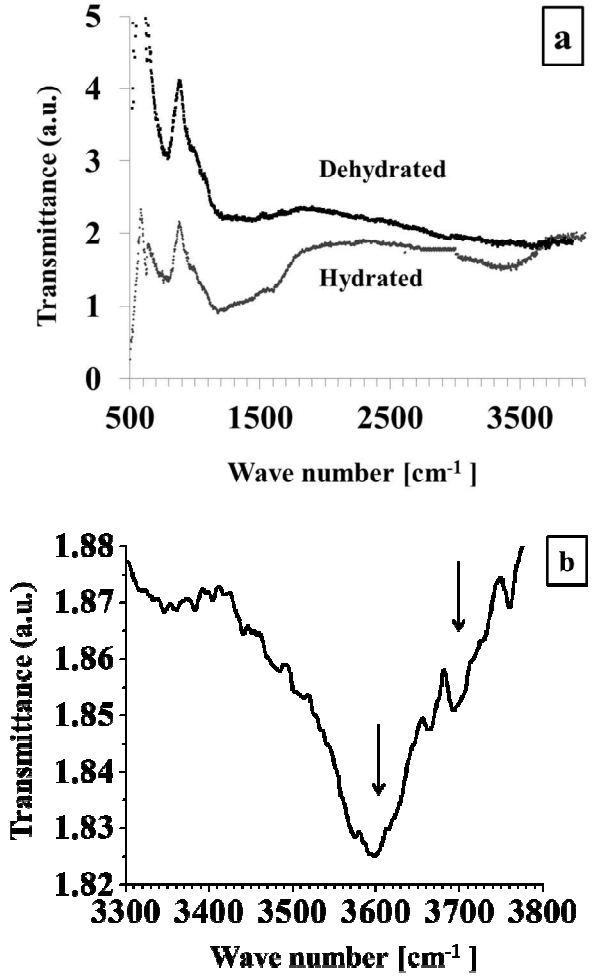

Fig. 9. DRIFTS spectra of the hydrated and dehydrated Pt/Y/V catalyst (a), and spectrum in the OH region (b).

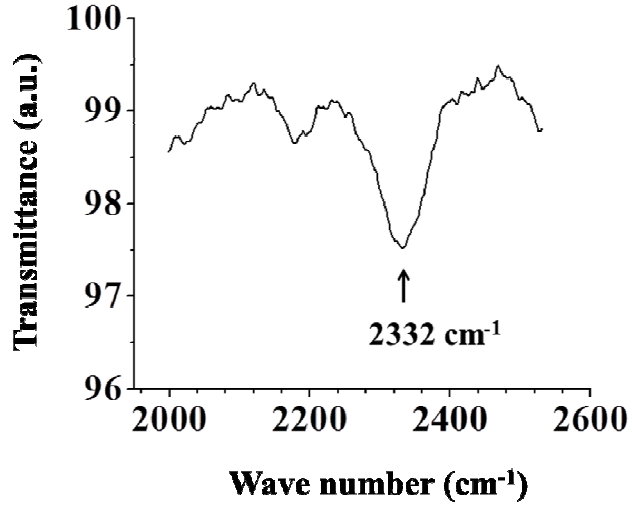

Fig. 10. DRIFTS spectrum of adsorbed carbon dioxide on the dehydrated zeolite contained in the Pt/Y/V catalyst.

The free carbon dioxide molecule belongs to the $D_{\infty h}$ group of symmetry, exhibiting four fundamental vibration modes, namely, the symmetric stretching, ν_1 (1338 cm^{-1}), the doubly degenerate bending vibration, ν_{2a} and ν_{2b} (667 cm^{-1}), and the asymmetric stretching vibration ν_3 (2349 cm^{-1}).[46] The, ν_2 and ν_3, modes are infrared active, whereas ν_1 is only Raman active in the free molecule.[47] The asymmetric stretching vibration, ν_3, of the adsorbed carbon dioxide molecule, at ca. at ca. 2332 cm^{-1} corresponds to carbon dioxide physically adsorbed inside the Y zeolite framework.[48]A red shift is observed the molecule is adsorbed. Note that 2349 is larger than 2332, indicating that the C=O bonding is weaker when the molecule is adsorbed.

As a final point of the present section was performed the fitting of the Dubinin-Radushkevitch (DR) adsorption isotherm equation[49], $\ln(n_a) = \ln(N_a) - (RT/\beta E)^2[\ln(P_0/P)]^2$, where, E, is a parameter known as the characteristic energy of adsorption, β, is the affinity coefficient, and, N_a, is the maximum amount adsorbed in the micropore volume, to the experimentally measured adsorption data, specifically, the amount adsorbed, n_a, at 273 K, of CO_2 on the Pt/V/Y catalyst and the inverse of the relative pressure, P_0/P, in the range, $0.002 < P/P_0 < 0.03$ [23]. The process allowed the calculation of the best fitting parameters, namely, N_a and E. After that, the micropore volume was computed using the Gurvich rule[19], i.e., $W_{MP} = N_a V_L$ where $V_L = 48.3\ cm^3/g$ is the carbon dioxide molar volume, yielding, $W_{MP}^{CO_2} = 0.105\ cm^3/g$. Then, since the micropore volume of pure zeolite Y is ca. 0.30 cm^3/g, subsequently, the amount of zeolite Y in the Pt/V/Y catalyst is ca. 0.33 ± 0.08 g/g[48], a quantity consistent with the TGA data.

3.2 KOH cyclic voltammetry and surface area determination

To properly assess the activity of an electro-catalyst, the currents produced as a result of the electrochemical reaction must be normalized, namely, calculated with respect to the real surface area in our case the electrochemical surface area (ECSA).[50] In this regard, in Figure 11 are reported the normalized cyclic-voltammetry curves corresponding to Pt/Y/V, NaY, Vulcan XC-72R, 40% Pt-Vulcan XC-72R (ETEK) and Pt black catalysts in 0.1 M KOH.

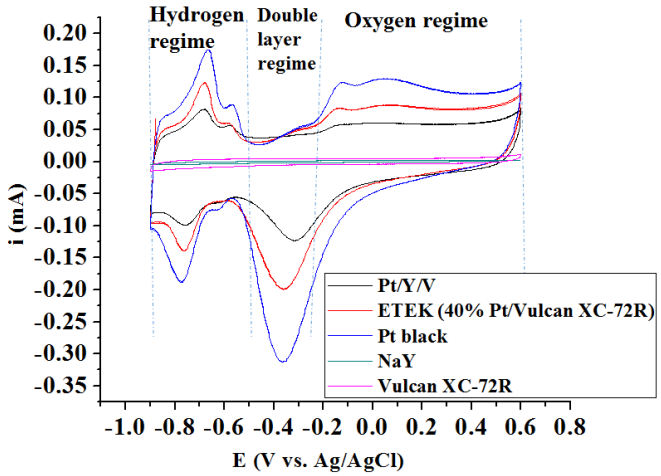

Fig. 11. Cyclic Voltammetry curves of Pt/Y/V, NaY, Vulcan XC-72R, 40% Pt-Vulcan XC-72R (ETEK) and Pt black catalysts in 0.1 M KOH.

The following reaction[51, 52], $Pt + H^+ + e^- \leftrightarrow Pt - H_{ad}$, describes hydrogen adsorption-desorption, in basic media, in the cathodic and anodic sections of the voltammograms. The characteristic hydrogen adsorption-desorption phenomena are manifested as peaks in the voltammograms, next, is found the double-layer effect, and, afterwards, the oxide formation peak is perceived. In the reported voltammograms evidence these features. Particularly, the hydrogen adsorption-desorption phenomena are notably informative, given that, platinum nanoparticles exhibit certain crystallographic planes at the surface, known as facets, displaying the (111), (100), and (110) indexes.[53,54,55] The presence of these facets induces in the voltammograms peaks location at different potentials. The principal shapes encountered for Pt nanoparticles are, tetrahedral-octahedral exhibiting the (111) and (110) basal planes, cubic exhibiting the (100), hexagonal exhibiting the (100) and (111) and near spherical nanoparticles exhibiting the (111) and (100) facets.[54,53] Hence, is possible to affirm that the peaks reported in Figure 9 are related to polycrystalline nanoparticles[56], given that, platinum nanoparticles normally tend to display a combination of (111) and (100) facets to reduce the particle interfacial free energy.

Meanwhile, the distinctive hydrogen adsorption-desorption phenomena in the Pt/Y catalyst were not clearly displayed as peaks in the voltammograms. This fact indicates that plain zeolite is an unsuitable support to produce an electro-catalyst. In other words, the presence of a conducting support is, in general, necessary in the catalyst formulation. Moreover, the capacitance was higher in the all catalysts with zeolites.

3.2 Methanol electrooxidation

The activity of Pt/Y/V, ETEK and Pt-black towards methanol oxidation in basic media: $CH_3\,OH + 6\,OH^- \rightarrow CO_2 + 5\,H_2O + 6\,e^-$, was investigated by cyclic voltammetry in degassed CH_3OH (1 M) - KOH (0.1 M) aqueous solutions (Fig. 12 and Table 2).

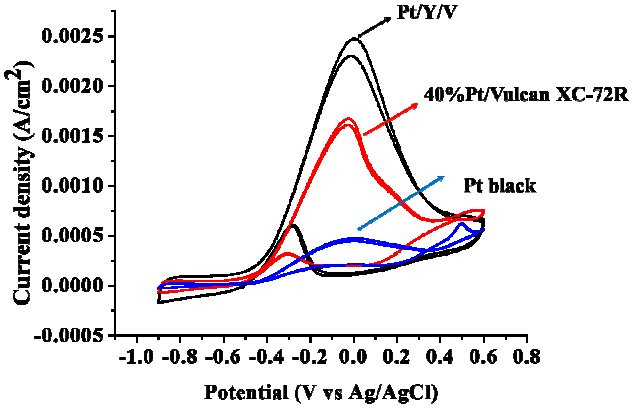

Fig. 12. Cyclic-voltammetry curves of Pt/Y/V, Pt black, and ETEK (40% Pt-Vulcan XC-72R) catalysts in degassed CH_3OH (1 M) - KOH (0.1 M) aqueous solutions.

The onset potential (E_s) for methanol oxidation is at -0.35 V vs. Ag/AgCl.

The maximum current densities of the three catalysts are 2.5 (Pt/Y/V), 1.7 (40 %Pt/Vulcan XC-72R), and 0.5 mA/ cm^2 of Pt (Pt black), respectively.

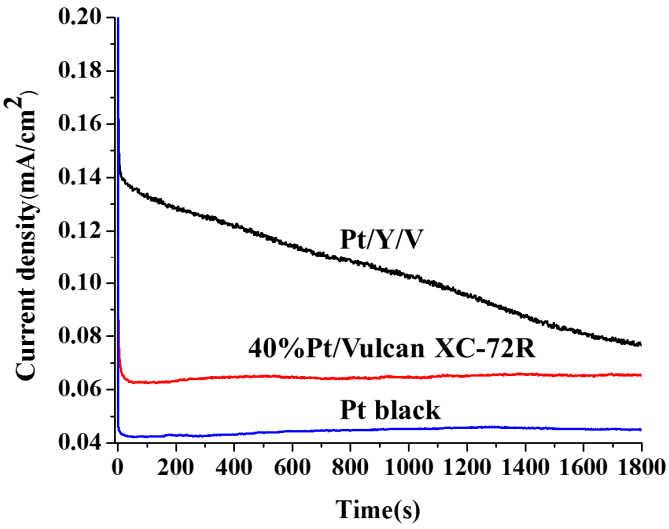

Fig. 13. Chronoamperometry of Pt/Y/V, 40% Pt/Vulcan XC-72R, and Pt black in 1.0 M CH_3OH/ 0.1 M KOH at an applied potential of -0.4 V vs. Ag/AgCl.

Fig. 13 shows the chronoamperometric experiments which was carried out to observe the stability and possible poisoning between the ETEK and Pt/Y/V under short time continuous operation toward methanol oxidation reaction. To measure the tolerance of the Pt/Y/V nanocatalysts to methanol oxidation reaction, it conducted chronoamperometry tests in 1.0 M CH_3OH/ 0.1 M KOH for 1800 s. As can been seen from Figure 10, the potentiostatic current decreases rapidly in the initial period of time; and this can be due to the formation of CO_{ads} and other intermediate species, such as CH_3OH_{ads}, CHO_{ads} and OH_{ads}, during methanol oxidation reaction. The Pt/Y/V seems to be clearly more stable because exhibit a tolerance for intermediate species formed during the methanol oxidation than the commercial catalysts.

3.3 CO stripping experiment

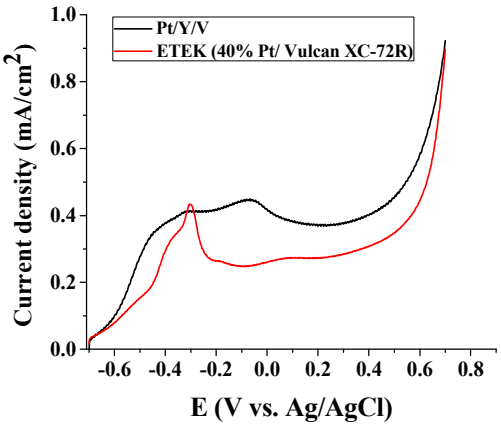

Fig. 14. CO stripping voltammograms of the NaY/Vulcan/Pt and 40% Pt/Vulcan XC-72R catalysts in 0.1 M KOH at 25 ◦C after full adsorption of CO and subsequent purging of the solution with high-purity Argon at a scan rate of 25 mV/s.

One of the principle facts to take in consideration at the time of doing characterization of the nanocatalysts material for fuel cells is the resistance of the CO poisoning. CO stripping voltammetry is commonly used to test the activity of a catalyst for electrochemically oxidizing adsorbed CO on the catalyst. In Fig. 14 shows the CO stripping voltammograms of the Pt/Y/Vulcan and 40% Pt/Vulcan XC-72R catalysts in 0.1 M KOH at 25 ◦C after full adsorption of CO and subsequent purging of the solution with high-purity Argon at a scan rate of 25 mV/s. CO stripping voltammetry is a technique used to calculate the Pt-CO saturated coverage at Pt. The charge required to oxidize the saturated CO layer on a NaY/ Vulcan/Pt was determined from the electrochemical CO desorption method and assuming a full CO-Pt coverage, which is used for Pt surface area determination. Basically, the CO adsorption method is the same as the hydrogen adsorption method i.e. a probe molecule is adsorbed at the Pt surface (at potential where CO oxidation does not occur). Pt catalysts supported on zeolite have been reported for the removal of CO, taking advantage of its "chemical and/or physical molecular sieve effect" to make CO react with oxygen.[23] In Fig.14 we see a lower CO stripping potential for Pt/Y/V than for 40% Pt/Vulcan XC-72R.

Another way to evaluate the electro-catalytic activity for methanol oxidation, the turnover number (TON) is normally used (Table 2).[57]

Table 2. Turnover number at maximum peak current in 1.0 M CH_3OH/ 0.1 M KOH for methanol oxidation

Catalyst	$TON_{Max}\left[\frac{molecules}{\sec \times site}\right]$	At Maximum Peak Current Potential [V versus Ag/AgCl]
Pt/Y/V	1.72	0.00
Pt-Black	1.10	-0.04
ETEK	0.34	-0.02

The TON is just the number of revolutions of the catalytic cycle per second, consequently is a parameter showing effects close to the atomic-molecular nature of the catalytic process. This parameter, in the concrete case of electro-catalytic methanol oxidation, is defined as the number of reacted methanol molecules per metallic catalytic site, in the catalyst surface within one second. The turnover number is estimated, using the maximum oxidation peak current in the cyclic voltammogram, with the following relation:[58,5]

$$TON = \frac{I[mA/cm^2]}{n \times e[C] \times N_{Pt}[1/cm^2]} \quad \left[\frac{molecules}{\sec ond \times site}\right] \qquad (1)$$

Where, *I,* is the maximum steady-state current density, e=1.602x10^{-19} *C,* is the elementary charge of the electron, n=6, is the number of electrons generated by the one mol of methanol in the course of the electrochemical oxidation reaction, and N_{Pt}[1/cm^2]=1.51x10^{15}/cm^2, is the mean atomic density of Pt(111) surface atoms.[59] In Table 2 are reported the TON calculated using equation "1" for the tested catalysts.

In the complex process produced during methanol oxidation, the extent of the anode peak current and the TON characterize the electro-catalytic activity of the catalyst toward methanol oxidation. In this regard, the Pt/Y/V catalyst exhibited current density and TON values higher for methanol oxidation than that of the Pt black and ETEK catalysts, although the surface area of the platinum black and ETEK catalysts are higher than that of the Pt/Y/V catalyst (Table 2).

3.4. Role of the zeolite included in the catalyst in the reaction mechanism

In the methanol oxidation electrochemical reaction many electrons are released, therefore, this whole process requires a complicated mechanism involving several steps, namely, adsorbed intermediates and side-products to be produced, then, if some of these intermediates are irreversibly adsorbed (e.g. CO) on the platinum catalyst the course of the reaction is hindered. In this regard, in both acid and basic media the oxidation of adsorbed *CO* may occur via the Langmuir−Hinshelwood mechanism:[60]

$$CO_{ad} + OH_{ad} \rightarrow CO_2 + H^+ + e^- \qquad (2)$$

Where, all the intermediate steps are fast, except *CO* removal, accordingly, the rate of the overall methanol oxidation may be controlled by this step. Therefore, the electro-catalytic activity is determined by the accumulation rate of adsorbed *CO* formed during methanol oxidation and their oxidation rate into CO_2. Within the frame of this mechanism was supposed that carbon black act merely as a support.[56] In contrast, it is accepted that the physical properties of the support influence the performance of the catalyst, promoting dispersion of the platinum nanoparticles and enabling the electron transfer.[7]

The main result evidenced by Fig. 12 and Table 2 is that the Pt/Y/V catalyst presented a high activity towards methanol oxidation when compared to Pt black and ETEK. This fact should be related to this catalyst lower CO poisoning. To explain this finding is necessary to take into account that Y zeolite is an excellent adsorbent in gaseous and as well in liquid phase[61], therefore, is reasonable to suppose that the mechanism producing the high activity of the Pt/V/Y catalyst is CO_2 adsorption by the zeolite phase included in the catalyst formulation, given that, the removal of this molecule promote the oxidation of adsorbed *CO* (equation "2"). However, carbon dioxide interacts with water, according to the following equilibrium reaction, $CO_2 + H_2O \leftrightarrow HCO_3^- + H^+$, on this ground, the zeolite should adsorb solvated molecular carbon dioxide and bicarbonate anions.

The framework of zeolite Y is composed of sodalite cages, linked by 6-6 secondary building units, located in a face centered cubic lattice, where half of the tetrahedral sites are occupied by sodalite cages as is the case in the structure of diamond.[30,31] This framework, known as FAU type, contains 12-member rings (MR) windows which lead to approximately spherical cavities, with a radius of R = 6.9 Å, known as β cages, that are connected in tetrahedral symmetry, and opened though four 12-member rings (MR) windows each one with a diameter of d = 7.4 Å.[62] When the solvated carbon dioxide and bicarbonate molecules are immersed in the Y zeolite adsorption space[31] they become subjected to diverse interaction fields, such as, the dispersion, repulsion energies, the electrostatic interactions, namely, polarization, field dipole and field gradient quadrupole interactions[48] and the adsorbate-adsorbate

interaction.[63] On this ground, the structure and surface chemistry of the H-Y zeolite, included in the catalyst, allows carbon dioxide adsorption in liquid phase. This fact explains why the Pt/Y/V catalyst is more active than both the Pt black and ETEK catalysts.

In general, to reduce the CO poisoning problem the platinum catalyst is alloyed with Ru, Sn, W, Mo, and other metals oxides to produce bifunctional sites in the catalyst surface.[32] On the surface of this alloy, the Pt sites are centers for CO adsorption and dehydrogenation, while on the other metallic sites present in the alloy nanoparticles surface, the OH_{ad} adsorbed species react with the adsorbed CO_{ad} to produce, CO_2, in consequence, the CO poisoning species is detached from the catalyst.[64] Platinum-ruthenium alloys nanoparticles are considered the most active electro-catalysts for methanol oxidation.[65] Conversely, ruthenium is expensive, hence the tested catalyst may open an avenue for the formulation of efficient and low-priced methanol oxidation Pt based catalysts.

4. Conclusions

The electro-deposition of the platinum catalyst nanoparticles was performed using the RoDSE technique on Y zeolite and Y zeolite/Vulcan composite supports. The catalyst materials were characterized with electron microscopy, X-ray photoelectron spectrometry, powder X-ray diffraction, thermo-gravimetric analysis, diffuse reflectance Fourier transform infrared spectrometry and carbon dioxide adsorption.

TEM showed the presence of Pt nanoparticles and Pt tetrahedral, morphology due to the zeolite framework on nucleation. The XPS data revealed that the majority of the platinum was in its metallic form indicating that the deposition process was very efficient. The TGA, DRIFTS and adsorption data demonstrated that the zeolite included in the Pt/Y/V catalyst conserved their structure after all the treatments suffered by this materials, then exhibiting a microporous channel system containing acid bridging hydroxyls on their surface.

The voltammograms corresponding to Pt/Y/V, 40 wt.% Pt/ Vulcan XC-72R, and Pt black catalysts exhibited a similar behavior. In basic media, the Pt/Y/V catalyst exhibited current density values significantly higher for methanol oxidation than that of the 40 wt.% Pt/Vulcan XC-72R, and Pt black catalysts. Since, it is acknowledged that the electro-catalytic activity for the tested process is determined by the accumulation rate of adsorbed *CO*, and the H-Y zeolite is an excellent adsorbent, consequently, is rational to assume that the mechanism producing the high activity of the Pt/V/Y catalyst is CO_2 adsorption by the zeolite phase included in the catalyst formulation.

The platinum catalyst is normally alloyed with Ru, Sn, W, Mo, and other metals to produce bifunctional sites in the catalyst surface and reduce the CO poisoning. Platinum-ruthenium alloys nanoparticles are considered the most active electro-catalysts for methanol oxidation; however ruthenium is very expensive in comparison to a Na-Y zeolite. Consequently, the inclusion of a zeolite in the electro-catalyst opens an avenue for the design of catalysts that may reduce CO poisoning.

Acknowledgments

This work was partially funded by NASA-URC Grant Number NNX10AQ17A. The authors R.P. and R.R.M. (University of Turabo) acknowledge the financial support provided by the US Department of Energy through the Massey Chair project and the National Science Foundation (CHE-0959334). We thank Ms. Frances Lugo, Mr. Ian Gutierrez Molina, Mr. Carlos Muñiz and the Puerto Rico Energy Center. NSF for its support (award 0701525) to the Nanoscopy Facility, an electron microscopy facility at UPR.

Notes and references

[a] *Department of Chemistry and Molecular Sciences Research Building, University of Puerto Rico, 1390 Ponce De León Ave. Suite 2, San Juan, Puerto Rico 00926, USA. E-mail: carlos.cabrera2@upr.edu*

[b] *Institute for Physical Chemical Applied Research, School of Science, University of Turabo, PO Box 3030, Gurabo, PR, 00778-3030, USA. E-mail: rroque@suagm.edu*

[c] *Department of Physical Sciences, General Studies College, University of Puerto Rico, Río Piedras Campus, JBR Blgd., of. # 353, San Juan, Puerto Rico 00931, USA.*

[d] *Department of Physics, University of Puerto Rico, San Juan, Puerto Rico 00931, USA.*

References

1. P. Jena, *Journal of Physical Chemistry Letters*, 2011, 2, 206-211.
2. H. S. Wang and H. D. Abruna, in *Fuel Cells and Hydrogen Storage*, eds. A. Bocarsly and D. M. P. Mingos, 2011, vol. 141, pp. 33-83.
3. D. Chu and R. Z. Jiang, *Solid State Ionics*, 2002, 148, 591-599.
4. C. Bianchini and P. K. Shen, *Chemical Reviews*, 2009, 109, 4183-4206.
5. E. H. Yu, U. Krewer and K. Scott, *Energies*, 2010, 3, 1499-1528.
6. R. Z. Jiang and D. R. Chu, *Journal of the Electrochemical Society*, 2004, 151, A69-A76.
7. E. Antolini, *Applied Catalysis B-Environmental*, 2009, 88, 1-24.
8. A. D. Moore, S. M. Holmes and E. P. L. Roberts, *Rsc Advances*, 2012, 2, 1669-1674.
9. S. C. Thomas, X. M. Ren, S. Gottesfeld and P. Zelenay, *Electrochimica Acta*, 2002, 47, 3741-3748.
10. E. Antolini, *Mater. Chem. Phys.*, 2003, 78, 563-573.
11. S. Wasmus and A. Kuver, *Journal of Electroanalytical Chemistry*, 1999, 461, 14-31.
12. X. L. Sui, Z. B. Wang, M. Yang, L. Huo, D. M. Gu and G. P. Yin, *Journal of Power Sources*, 2014, 255, 43-51.
13. D. Santiago, G. G. Rodriguez-Calero, H. Rivera, D. A. Tryk, M. A. Scibioh and C. R. Cabrera, *Journal of the Electrochemical Society*, 2010, 157, F189-F195.
14. D. Santiago, G. G. Rodriguez-Calero, A. Palkar, D. Barraza-Jimenez, D. H. Galvan, G. Casillas, A. Mayoral, M. Jose-Yacaman, L. Echegoyen and C. R. Cabrera, *Langmuir*, 2012, 28, 17202-17210.
15. W. Z. Li, C. H. Liang, J. S. Qiu, W. J. Zhou, H. M. Han, Z. B. Wei, G. Q. Sun and Q. Xin, *Carbon*, 2002, 40, 791-794.
16. C. M. Chang, H. Y. Li, J. Y. Lai and Y. L. Liu, *Rsc Advances*, 2013, 3, 12895-12904.
17. G. S. Chai, S. B. Yoon, J. S. Yu, J. H. Choi and Y. E. Sung, *Journal of Physical Chemistry B*, 2004, 108, 7074-7079.

18. L. La-Torre-Riveros, R. Guzmán-Blas, A. E. Mendez-Torres, M. Prelas, D. A. Tryk and C. R. Cabrera, *Acs Applied Materials & Interfaces*, 2012, 4, 1134-1147.
19. K. V. Kordesch and G. R. Simader, *Chemical Reviews*, 1995, 95, 191-207.
20. T. M. Salama, I. O. Ali and H. A. Gumaa, *Microporous Mesoporous Mat.*, 2008, 113, 90-98.
21. Z. Tang, J. Monroe, J. Dong, T. Nenoff and D. Weinkauf, *Industrial & Engineering Chemistry Research*, 2009, 48, 2728-2733.
22. P. Kaminski, I. Sobczak, P. Decyk, M. Ziolek, W. J. Roth, B. Campo and M. Daturi, *The Journal of Physical Chemistry C*, 2013, 117, 2147-2159.
23. D. R. Rolison and C. A. Bessel, *Accounts of Chemical Research*, 2000, 33, 737-744.
24. D. R. Rolison, *Chemical Reviews*, 1990, 90, 867-878.
25. D. R. Rolison, *Advanced Zeolite Science and Applications*, 1994, 85, 543-586.
26. M. Hernandez-Vélez and R. Roque-Malherbe, *Journal of Materials Science Letters*, 1995, 14, 1112-1114.
27. T. M. Mudrinić, Z. D. Mojović, A. Z. Ivanović-Šašić, N. S. Vukelić, Ž. D. Čupić and D. M. Jovanović, *Russ. J. Phys. Chem.*, 2013, 87, 2127-2133.
28. O. Vigil, J. Fundora, H. Villavicencio, M. Hernandez-Velez and R. Roque-Malherbe, *Journal of Materials Science Letters*, 1992, 11, 1725-1727.
29. R. Roque-Malherbe, *Adsorption and Diffusion in Nanoporous Materials, CRC Press, Boca Raton, FL, USA*, 2007.
30. D. W. Breck, *Zeolite Molecular Sieves, Wiley-Interscience, J. Wiley & Sons, New York*, 1974.
31. R. Roque-Malherbe, *CRC Press, Boca Raton, FL, USA*, 2009.
32. G. R. Li, H. Xu, X. F. Lu, J. X. Feng, Y. X. Tong and C. Y. Su, *Nanoscale*, 2013, 5, 4056-4069.
33. M. C. Silaghi, C. Chizallet and P. Raybaud, *Microporous Mesoporous Mat.*, 2014, 191, 82-96.
34. T. C. Gruber, T. W. Zerda and M. Gerspacher, *Carbon*, 1993, 31, 1209-1210.
35. G. Selvarani, S. V. Selvaganesh, S. Krishnamurthy, G. V. M. Kiruthika, P. Sridhar, S. Pitchumani and A. K. Shukla, *Journal of Physical Chemistry C*, 2009, 113, 7461-7468.
36. R. L. Barbosa, V. Papaefthimiou, Y. T. Law, D. Teschner, M. Havecker, A. Knop-Gericke, R. Zapf, G. Kolb, R. Schlogl and S. Zafeiratos, *Journal of Physical Chemistry C*, 2013, 117, 6143-6150.
37. D. C. Higgins, D. Meza and Z. W. Chen, *Journal of Physical Chemistry C*, 2010, 114, 21982-21988.
38. R. Roque-Malherbe, O. N. C. Uwakweh, C. Lozano, R. Polanco, A. Hernandez-Maldonado, P. Fierro, F. Lugo and J. N. Primera-Pedrozo, *Journal of Physical Chemistry C*, 2011, 115, 15555-15569.
39. J. W. Arblaster, *Platinum Metals Rev.*, 1997, 41, 12-21.
40. X. W. Yu and S. Y. Ye, *Journal of Power Sources*, 2007, 172, 133-144.
41. M. M. Treacy and J. B. Higgins, *Elsevier, Amsterdam*, 2001.
42. A. Dyer, *Thermochimica Acta*, 1987, 110, 521-526.
43. W. Martinez, T. T. Thompson and M. A. Smit, *International Journal of Electrochemical Science*, 2010, 5, 931-943.
44. H. Knozinger and S. Huber, *Journal of the Chemical Society-Faraday Transactions*, 1998, 94, 2047-2059.
45. J. Matthey, http://www.chemicals.matthey.com/userfiles/files/Pt(1).pdf, 2009.
46. A. Zecchina and C. O. Arean, *Chemical Society Reviews*, 1996, 25, 187-&.
47. J. A. Lercher, C. Grundling and G. EderMirth, *Catalysis Today*, 1996, 27, 353-376.
48. R. Roque-Malherbe, R. Polanco-Estrella and F. Marquez-Linares, *Journal of Physical Chemistry C*, 2010, 114, 17773-17787.
49. B. P. Bering, M. M. Dubinin and V. V. Serpinsky, *J. Coll. Int. Sci.*, 1972, 38, 185-194.
50. S. Trasatti and O. A. Petrii, *Pure and Applied Chemistry*, 1991, 63, 711-734.
51. C. Korzeniewski, V. Climent and J. M. Feliu, *Electroanalytical Chemistry: A Series of Advances, Vol 24*, 2012, 24, 75-169.
52. N. M. Markovic and P. N. Ross, *Surface Science Reports*, 2002, 45, 121-229.
53. C. M. Sanchez-Sanchez, J. Solla-Gullon, F. J. Vidal-Iglesias, A. Aldaz, V. Montiel and E. Herrero, *Journal of the American Chemical Society*, 2010, 132, 5622-+.
54. R. Narayanan and M. A. El-Sayed, *Nano Letters*, 2004, 4, 1343-1348.
55. B. Lim, M. J. Jiang, P. H. C. Camargo, E. C. Cho, J. Tao, X. M. Lu, Y. M. Zhu and Y. N. Xia, *Science*, 2009, 324, 1302-1305.
56. J. Solla-Gullon, F. J. Vidal-Iglesias, A. Lopez-Cudero, E. Garnier, J. M. Feliu and A. Aldaza, *Physical Chemistry Chemical Physics*, 2008, 10, 3689-3698.
57. J. Kim, C. Jung, C. K. Rhee and T. H. Lim, *Langmuir*, 2007, 23, 10831-10836.
58. E. Herrero, K. Franaszczuk and A. Wieckowski, *Journal of Physical Chemistry*, 1994, 98, 5074-5083.
59. L. Li and Y. C. Xing, *Energies*, 2009, 2, 789-804.
60. N. M. Markovic, C. A. Lucas, B. N. Grgur and P. N. Ross, *Journal of Physical Chemistry B*, 1999, 103, 9616-9623.
61. C. Muñiz-López, J. Duconge and R. Roque-Malherbe, *Journal of Colloid and Interface Science*, 2009, 329, 11-16.
62. R. F. Lobo, *Handbook of Zeolite Science and Technology, S.M. Auerbach, K.A. Carrado, P.K. Dutta (Eds.), Marcell Dekker Inc., New York*, 2003, 65-69.
63. R. Roque-Malherbe and F. Diaz-Castro, *Journal of Molecular Catalysis a-Chemical*, 2008, 280, 194-202.
64. H. S. Wang, L. R. Alden, F. J. DiSalvo and H. D. Abruna, *Langmuir*, 2009, 25, 7725-7735.
65. S. L. Gojkovic, T. R. Vidakovic and D. R. Durovic, *Electrochimica Acta*, 2003, 48, 3607-3614.

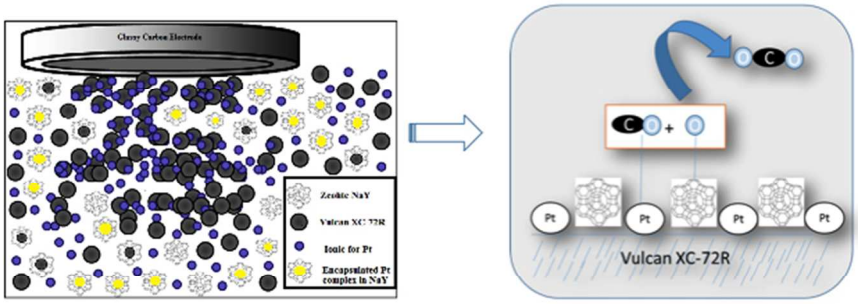

254x142mm (72 x 72 DPI)